

# Model-based Region-of-interest Selection in Dynamic Breast MRI

Florence Forbes, PhD,\* Nathalie Peyrard, PhD,† Chris Fraley, PhD,‡ Dianne Georgian-Smith, MD,§ David M. Goldhaber, PhD,|| and Adrian E. Raftery, PhD¶

**Abstract:** Magnetic resonance imaging (MRI) is emerging as a powerful tool for the diagnosis of breast abnormalities. Dynamic analysis of the temporal pattern of contrast uptake has been applied in differential diagnosis of benign and malignant lesions to improve specificity. Selecting a region of interest (ROI) is an almost universal step in the process of examining the contrast uptake characteristics of a breast lesion. We propose an ROI selection method that combines model-based clustering of the pixels with Bayesian morphology, a new statistical image segmentation method. We then investigate tools for subsequent analysis of signal intensity time course data in the selected region. Results on a database of 19 patients indicate that the method provides informative segmentations and good detection rates.

**Key Words:** image segmentation, region of interest selection, magnetic resonance imaging, MR mammography, dynamic contrast-enhanced breast MRI, time-signal intensity curves, model-based clustering, Bayesian morphology

(*J Comput Assist Tomogr* 2006;30:675–687)

Magnetic resonance imaging (MRI) is emerging as a powerful tool for the diagnosis of breast abnormalities. Its unique ability to provide morphological and functional information can be used to assist in the differential diagnosis of lesions that other methods find questionable. Many studies have demonstrated the usefulness of MRI in the evaluation of the extent of breast cancer and in treatment planning. It is currently viewed as a complementary diagnostic modality in breast imaging. A number of recent surveys treat breast MRI issues.<sup>1–5</sup>

Because of the high reactivity of breast carcinomas after gadolinium injection, MRI has the potential to allow differentiation between malignant and benign tissues. However, there are as yet no firm standards for data acquisition, post-

processing, image analysis, and interpretation of dynamic breast MRI results.

It is well known that some benign lesions also enhance, as a result reducing the specificity of MRI. Several methods have been investigated to improve the discrimination between benign and malignant lesions. Lexicons have been designed to standardize the rating and reporting of lesions depicted on magnetic resonance (MR) images and to reduce inter- and intraobserver variability.<sup>6</sup> Improvements have also been achieved through development of contrast agents and pharmacokinetic models. The ultimate goal is to produce sophisticated computer-aided diagnostic tools combining an expanding knowledge base of expert information with state-of-the-art algorithmic techniques for lesion localization, visualization, and classification.<sup>7–12</sup>

In the current study, we focus more specifically on region-of-interest (ROI) selection via dynamic analysis of the temporal pattern of contrast uptake to improve specificity. The criteria that are in use for differential diagnosis can be divided into those related to lesion enhancement kinetics and those related to lesion morphology. Signal intensity time course data are useful for differentiating benign from malignant enhancing lesions. The overall shape of the time-signal intensity curve is an important criterion, whereas a single attribute of the curve, such as the enhancement rate, may not be enough.

The evaluation of morphological features and the extraction of architectural information is usually also based on postcontrast images of enhancing areas, integrating qualitative with quantitative diagnostic criteria. Selecting an ROI is an important first step in the process of examining the contrast uptake characteristics of a breast lesion. However, no standard method for ROI selection and analysis of dynamic breast MR data has yet been established.

As regards tissue classification, there has been considerable research in brain MRI. Many methods are based on modeling the image intensity with a Gaussian mixture model via the Expectation–Maximization algorithm.<sup>13</sup> Extensions and variations allow the integration of spatial information into the classification process, using Markov random fields.<sup>14,15</sup> However, there are differences in the analysis of breast MRI and brain MRI, and less research has been devoted to the former. In breast MRI analysis, image segmentation (e.g., finding the ROI) is central. Also breast tissues are much more heterogeneous than brain tissues: normal breasts can consist almost entirely of fatty tissues or include extremely dense fibroglandular tissues, resulting in additional challenges for the analysis of breast MRI. In dynamic breast MRI, the information to be modeled at each

From the \*équipe MISTIS, Inria Rhône-Alpes, ZIRST, 655 av. de l'Europe, Montbonnot, 38334 Saint Ismier Cedex, France; †Biometrics and Artificial Intelligence Department of INRA, Domaine Saint Paul, site Agroparc, 84914 Avignon cedex 9, France; ‡Department of Statistics, University of Washington, Seattle WA; §Harvard Medical School, Department of Radiology, Massachusetts General Hospital, Boston, MA; ||International MRI Accreditation Resources, South San Francisco, CA; ¶Department of Statistics, University of Washington, Seattle WA.

Received for publication December 13, 2005; accepted February 1, 2006. Reprints: Chris Fraley, PhD, University of Washington (e-mail: fraley@stat.washington.edu).

Copyright © 2006 by Lippincott Williams & Wilkins

pixel is not a single intensity measure, but a signal intensity time curve.

In this article, we propose an unsupervised ROI selection method based on statistical techniques. We describe a multivariate classification method that enables us to take account of multiple measurements in a single analysis. We then produce classification images in which parts of the breast with similar signal intensity time courses are assigned to a class represented by a color. The resulting morphological information can be used to select an ROI by focusing on the pixels with the strongest enhancement. We have also developed some tools for analyzing the enhancement kinetics for pixels in the selected region.

In the following section, we describe our data set for this study. In the third section, we present the multivariate classification method. We describe the model-based clustering method, along with complementary procedures to include spatial information. In the fourth section, we discuss how to use the resulting classifications for ROI selection and enhancement

kinetics analysis, and we also propose techniques for improving differential diagnosis based on the shapes of the curves in the selected region. The procedure is then illustrated and the results for our data set reported in the fifth section.

## DATA

We considered sequences of images for 19 patients representing different cases (malignant and benign lesions). The data was acquired in an earlier study to evaluate lesions identified by conventional imaging (mammography and/or sonography) as requiring histological diagnosis.

The dynamic MRI protocol was a 2-dimensional field echo with repetition time  $TR = 120\text{--}200$  ms, echo time  $TE = 5$  ms, flip angle = 70 degrees, slice thickness = 11 mm, field of view  $FOV = 18\text{--}24$  cm, acquisition matrix =  $128 \times 256$ . This was done on a Toshiba OpArt 0.35T scanner.

Several 2-dimensional slices were available for each patient. For each slice, 25 sequential MR breast images were acquired (1 image approximately every 10 sec). See Figure 1

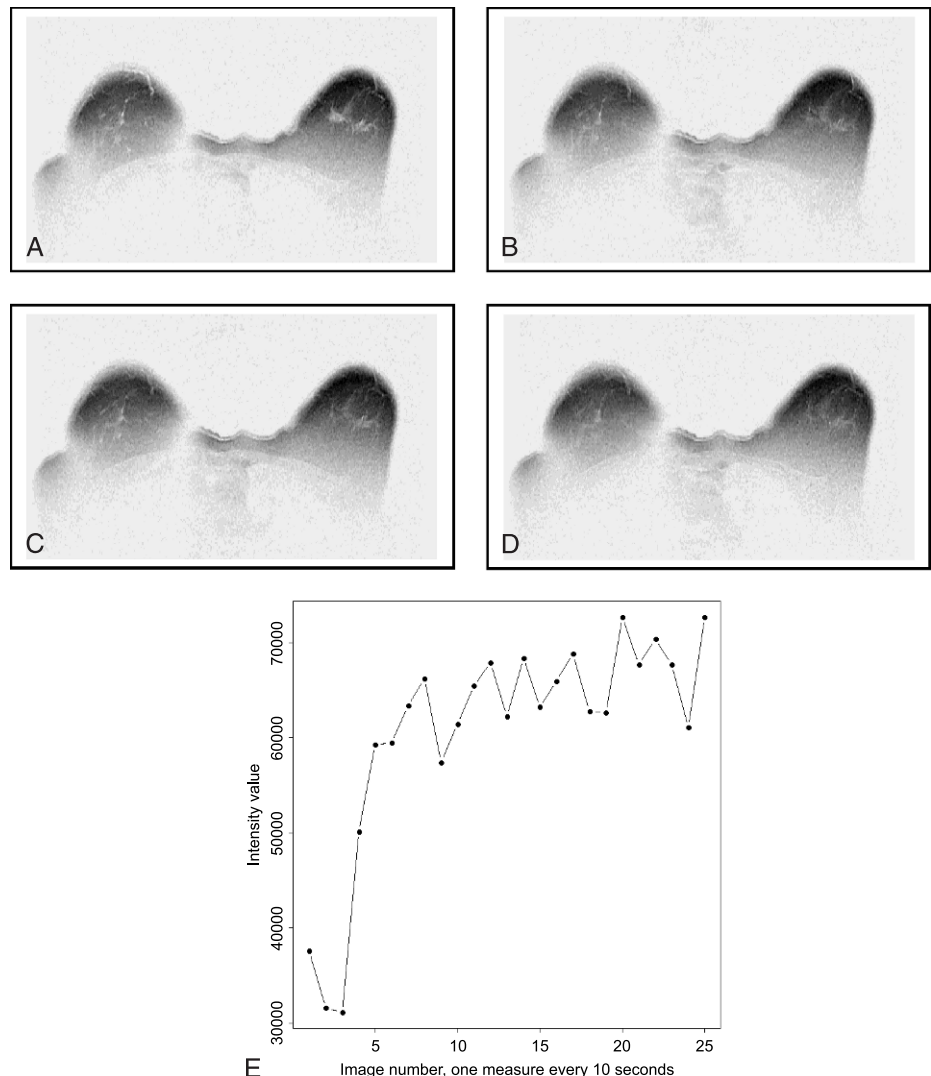


**FIGURE 1.** Patient 05, slice 09: dynamic MR images at (A) 10 seconds, (B) 70 seconds, (C) 150 seconds, (D) 250 seconds, (E) signal intensity curve at a given pixel, 25 measures were acquired, one measure every 10 seconds.

for examples of such images. Each image records the signal intensity at a given time after injection.

Instead of working directly with these MR images, we summarized them in terms of 5 derived variables considered to be of significance for cancer diagnosis. These 5 variables were calculated from a curve fitting procedure developed at Toshiba America MRI, Inc.<sup>16</sup> A fit analysis is carried out at each pixel location for the signal intensity curve. Figure 1E shows a signal intensity curve at a given pixel, after subtraction of the reference signal. The fitting model is assumed to be made of 3 successive sections: a zero signal, a second-order polynomial curve, and a flat line.

We used the following 5 derived variables in our study:

- *Time to Peak*: the time at which the signal peaks.
- *Difference at peak*: absolute increase of intensity between the beginning of the signal and the time at which the signal peaks.
- *Enhancement slope*: in units of intensity/time.
- *Maximum step*: maximum change between 2 adjacent dynamic samples.
- *Washout slope*: in units of intensity/time.

In addition to the images, diagnostic information is available. MRI-pathologic correlations were performed as part of the earlier study in which the data was acquired. All patients had tissue available. The core biopsies and hence the pathology results were obtained under MR guidance of the lesions that were identified, so the truth with regards to the tissues has been established. The core biopsies were all obtained within a month of the diagnostic MR imaging. Among the 19 patients, 12 have tumors diagnosed as carcinomas and 5 are diagnosed as not having cancer. For 2 others, the diagnosis is ambiguous. See the section on results for more details. We note that our study is limited to the determination of feasibility for our proposed computational methods; assessment of clinical value would entail a much more extensive and controlled study.

Our starting point is thus 5 images for each case, one showing the values of each derived variable at each pixel location, rather than the original 25 images. Although this preprocessing reduces the amount of data to be analyzed, the characterization of breast lesions based on these MR images remains a difficult task. In the next section, we present the multivariate statistical methods for clustering and spatial segmentation we propose to synthesize the available information into a single classification image.

### PRODUCING CLASSIFICATION IMAGES

We propose to use statistical segmentation methods to produce a color image for each case, in which each color represents a group or class of pixels with similar time-signal intensity curves (summarized by the 5 derived variables). An important issue is the determination of the effective number  $K$  of components present in the data, that is the number of colors to use in the classification image. The main components in the breast are blood vessels, air, fat, a possible tumor, and other tissues of less interest. Because of the large number of pixels involved, those corresponding to air are eliminated before

further analysis, leaving 3 or 4 components, depending on whether there is a tumor. We therefore, considered segmentations into 3 or 4 classes.

We also investigated the possibility that allowing more than 4 classes may provide better statistical performance in identifying the main features of interest in the image. We used a statistical method, Bayesian Information Criterion (BIC),<sup>17</sup> to determine the number of classes based on the data. The BIC is computed given the data and a model, and allows comparison of models with differing parameterizations and/or differing number of classes. It is the value of the maximized model loglikelihood with a penalty for the number of parameters in the model, and can be viewed as providing an approximation to the Bayes factor, which is the standard Bayesian approach to model selection.<sup>18</sup> Other statistical approaches to model selection have been proposed in the literature (e.g., Ref.<sup>19</sup>). BIC has become quite popular due to its simplicity and good results.

However, in our application, BIC tended to select values of  $K$  between 10 and 15, which accurately reflects the inhomogeneity of some kinds of tissue, but turned out not to help identifying tumors. In what follows, we have reported results for  $K = 3, 4,$  and  $10$ . Overall, we found that using  $K = 4$ , as suggested by the underlying biology, performed best.

Model-based statistical methods for clustering multivariate observations are flexible and have been widely applied.<sup>19,20</sup> However, for complex data, such as those associated with tissue segmentation in medical imaging, these methods can produce somewhat noisy results that do not correspond directly to a meaningful classification, because they do not take spatial dependence into account. For this reason, we propose refining the clustering results with a spatial statistical technique called Bayesian morphology.<sup>21</sup> Small isolated regions are removed by automatically reassigning pixels located in them, reducing the spatial fragmentation of the classification.

### Model-based Cluster Analysis

We propose to use *marginal mixture EM segmentation* as a first step in our analysis. The idea is to model the marginal distribution of (possibly multivariate) pixel intensities as a finite Gaussian mixture model, and use the EM (Expectation–Maximization) algorithm<sup>22</sup> to estimate the model parameters. The estimates were computed with the MCLUST software for model-based clustering.<sup>23</sup>

In what follows, observations (corresponding to image pixels) are denoted by  $y_i$  and are assumed to be 5-dimensional vectors, corresponding to the 5 derived variables. The  $y_i$  are assumed to arise from a  $K$ -component Gaussian mixture model so that if  $y_i$  belongs to class  $k \in \{1, \dots, K\}$ , its distribution is multivariate normal (Gaussian) with mean vector  $\mu_k$  and covariance matrix. The likelihood for our data is then

$$L(\Theta_1, \dots, \Theta_K; p_1, \dots, p_K | y) = \prod_{i=1}^n \sum_{k=1}^K p_k f_k(y_i | \Theta_k),$$

where  $\Theta_k = (\mu_k, \Sigma_k)$  and  $f_k$  is the multivariate normal density

of the  $k$ th component in the mixture, parameterized by its mean  $\mu_k$  and covariance matrix  $\Sigma_k$ :

$$f_k(y_i | \mu_k, \Sigma_k) = \frac{\exp\left\{-\frac{1}{2}(y_i - \mu_k)^T \Sigma_k^{-1} (y_i - \mu_k)\right\}}{\sqrt{\det(2\pi \Sigma_k)}}.$$

Here  $p_k$  is the probability that an observation belongs to the  $k$ th component ( $p_k \geq 0$ ;  $\sum_{k=1}^K p_k = 1$ ).

Data generated by mixtures of multivariate normal densities are characterized by groups or clusters centered at the means  $\mu_k$ . Geometric features (shape, volume, and orientation) of the clusters are determined by the covariances  $\Sigma_k$ , and the corresponding surfaces of constant density are ellipsoidal. Banfield and Raftery<sup>24</sup> proposed a general framework for geometric cross-cluster constraints in multivariate normal mixtures by parameterizing covariance matrices through eigenvalue decomposition in the form  $\Sigma_k = \lambda_k D_k A_k D_k^T$ , where  $D_k$  is the orthogonal matrix of eigenvectors,  $A_k$  is a diagonal matrix whose elements are proportional to the eigenvalues, and  $\lambda_k$  is an associated constant of proportionality. Their idea was to treat  $\lambda_k$ ,  $A_k$ , and  $D_k$  as independent sets of parameters, and either constrain them to be the same for each cluster or allow them to vary among clusters.

We obtained a first segmentation via MCLUST with the constant-shape model  $\Sigma_k = \lambda_k D_k A_k D_k^T$ . The algorithm provides an estimate of the conditional probability that each pixel belongs to each of the classes, given the observations. These probabilities are obtained using the EM algorithm. The segmentation derived from these conditional probabilities is the one which assigns each pixel to the class with the greatest probability.

## SPATIAL CLASSIFICATION

In the following subsections, we discuss refinements of our model-based classification to incorporate spatial information. In *Morphological Filters*, we describe image smoothing via morphological filters, which treat each pixel in the initial classification only in the context of neighboring pixels. In *Bayesian Morphology*, we discuss methods that make use of the original data in addition to the initial model-based classification.

### Morphological Filters

*Morphological filters* are procedures that successively apply a morphological rank operator to each pixel and its neighbors until there are no further changes.<sup>25</sup> Each pixel is considered in conjunction with characteristics of its surrounding neighbors. A rank parameter  $r$  controls smoothing, which increases as the value of  $r$  decreases.

We refer to morphological filters as *blind restoration*, because they do not make use of the original data. Blind restoration can smooth the data considerably, eliminating clutter and extraneous minor features in the image. In our application, it may help isolate possible tumors from the initial MCLUST classification. However, in images in which the tumor is less clearly identified, any smoothing operation

runs the risk of eliminating the tumor altogether, and should probably be used only in conjunction with less smoothed images as well. The appropriate images can be obtained using the procedure described in the next section.

### Bayesian Morphology

In Ref. 21, we showed that the Iterated Conditional Modes (ICM) algorithm<sup>26</sup> could be formulated using morphological terminology and proposed *Bayesian morphology*, a procedure that combines the speed of mathematical morphology with the principled statistical basis of ICM. In Bayesian morphology, a succession of morphological rank operators is applied, and at each iteration, the rank is estimated from the data and a current classification. An advantage is that conditions on the model parameters can be found that yield a segmentation that is not sensitive to their precise values. We use this fact to reduce the complexity of the estimation step in traditional unsupervised ICM, resulting in considerable savings in computation time. When performed on discrete images (or if an initial segmentation has been carried out), the resulting algorithm is equivalent to ICM in the sense that the final segmentation or classification is the same. In this case, it differs from ICM essentially in the way the parameter estimation step is carried out. According to the insensitivity conditions, point estimates need not be computed.

By estimating the rank of the morphological operator at each iteration instead of using a predetermined or arbitrary chosen rank, these methods make more use of the available information than blind restoration, and as a result tend to produce classifications with more detail. In comparison to blind morphology, less noise is likely to be eliminated, whereas ambiguous features worthy of further consideration are more likely to be retained. These classifications provide a first tool for guiding diagnosis. Often the lesion is easily identified and the radiologist can be asked to select regions that are suspicious or otherwise of interest to be further examined. In the next section, we show that additional information is present in the data that can be used for a more automatic detection and localization of lesions of interest.

## REGION-OF-INTEREST SELECTION

We now propose a way to automatically select an ROI using the color classification images produced in the first part of our study. Our second step consists of studying the values of each of the 5 derived variables within each class, on the basis of which we propose an ROI selection. The analysis can then be carried out by looking at the shape of the ROI (morphological feature analysis) or at the curves (kinetics analysis) for pixels in a selected cluster or region to identify the nature of the lesion.

### Deciding Which Segments Are Regions of Interest

In breast MRI, lesions are usually identified because they enhance after intravenous injection. In our study, we



focus on rapidly and strongly enhancing lesions, because malignant lesions tend to enhance more quickly than benign ones. Strong enhancements are characterized by a large *difference at peak*, that is the absolute increase in intensity between the beginning of the signal and the time at which the signal peaks. For a given classification image, the mean value of *difference at peak* is computed for each class in the image. We then select the class with the largest mean value as containing the ROI, and we identify the ROI as the biggest connected component in the class, as for instance in Figure 2E.

The difference at peak can also be used to determine a meaningful color assignment. In most classification methods, images are produced using colors (or equivalently class labels) artificially assigned to the different regions (see Table 1). In our study, we propose to automatically display our results using the highest difference at peak criterion so that suspicious regions can be marked with a predetermined label and always displayed with a specific color (e.g., red).

### Enhancement Kinetics Analysis

In diagnosis, an important point is to produce a *good* estimated pattern of uptake which should be representative of the lesion under study. A first idea is to use the ROI and compute the mean of all signals in the region. This should get rid of some noise but may be biased if the region is too big. We could also select 1 or a few pixels in the ROI with the

highest probability. We investigated other ways to compute such *mean* curves using weights. The idea is to give more weight to pixels in the ROI which are typical of the lesion and less weight to pixels for which we are more uncertain. The question is then to find reasonably good weights as automatically as possible. We investigated weighting schemes based on the highest difference at peak values, as well as on the conditional probability estimates provided by MCLUST (see *Model-based Cluster Analysis*).

### Distinguishing Between Malignant and Benign Lesions

Assuming that we have assigned a representative curve to the lesion under study, our third step is then to focus on the shape of this curve. We take into account information from other sources as in.<sup>27,28</sup> Three patterns of signal intensity curves are distinguished on the basis of 3 characteristics, the *enhancement rate*, the presence of a *plateau* and that of a *washout slope*. Type 1 shows a monophasic enhancement that persists until the late postcontrast period (linear time course). This type is indicative of a benign lesion. Type 2 is a biphasic enhancement in which signal intensity reaches the maximum approximately 2–3 minutes after injection and stays at this level (plateau curve). This type has been observed in both benign and malignant lesions. Type 3 is characterized by a washout enhancement. As in type 2, peak enhancement is already reached in the early postcontrast period but then it is

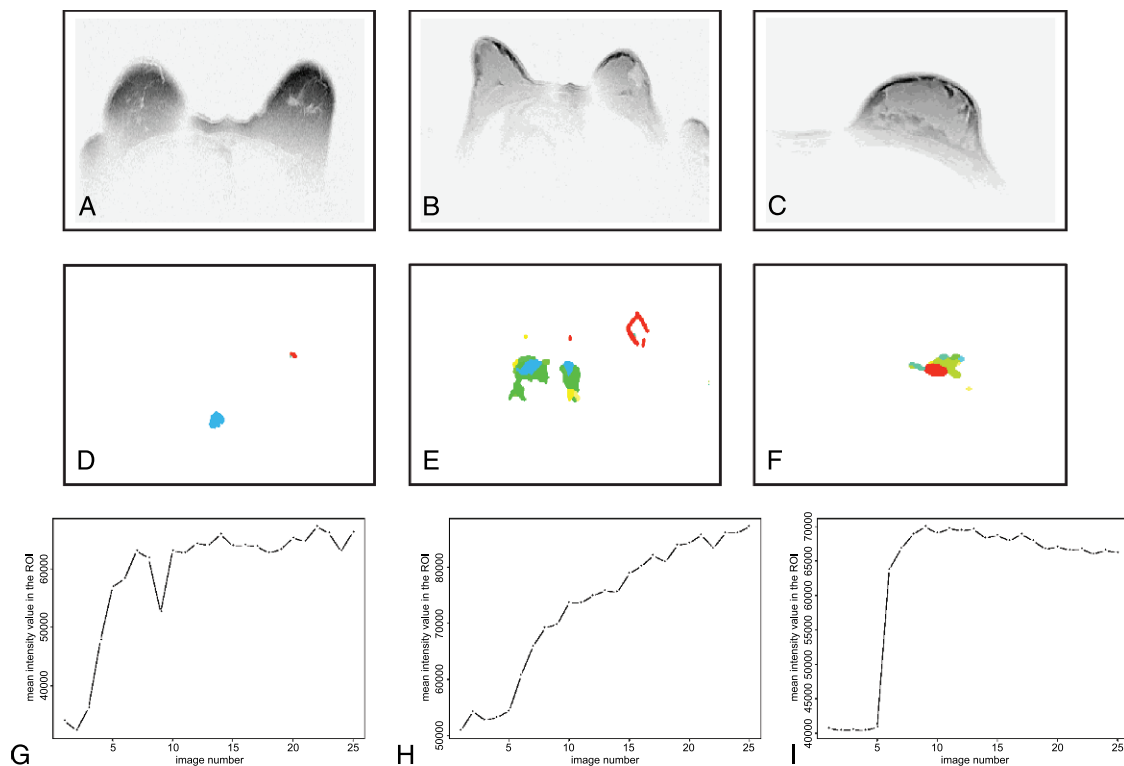


**FIGURE 2.** ROIs and associated mean curves in 3 cases. (A), (B), (C) dynamic image at  $t = 1$  for patient 05, slice 09, patient 08, slice 06 and patient 28, slice 10. (D), (E), (F) ROI selections (largest connected component in the red regions). (G), (H), (I) mean-time intensity signals in the ROIs.

**TABLE 1.** Patient 05, Slice 09

Patient 05 slice 09	Mean Difference at Peak	Mean Time to Peak	Interpretation
<i>K</i> = 3			
Class 2	10,363	-2061	Heart
Class 3	17,179	-4578	Lesion and skin
<i>K</i> = 4			
Class 2	13,006	-5468	Skin
Class 3	10,519	-1834	Heart
Class 4	27,068	-2819	Lesion
<i>K</i> = 10			
Class 8	29,840	-2222	Lesion (main)
Class 9	25,512	-3063	Lesion (border)
Class 10	9736	-1582	Heart

The classifications in the first column of Figure 3 into *K* = 3, 4, and 10 classes are used to compute mean values for variable *difference at peak* in each nonbackground component. The largest value corresponds to the lesion of interest whereas taking the largest mean *time to peak* would select the heart area.

followed by an intensity loss. A type 3 pattern strongly supports the diagnosis of a malignant breast tumor.

**RESULTS**

To assess the effectiveness of our procedure, we first focus on its ability to produce informative classification images (see *Breast MRI Segmentation*). In 3 cases, we illustrate in some detail the various choices of number of segments and segmentation methods that can be made. Summary ROI

analysis results (see *ROI Analysis*) are then given for all 19 patients (see Table 2). The ROIs in which the lesions in the MR scans were independently determined by a board certified, fellowship trained dedicated radiologist (DGS). A medical physicist (DMG) used this information to evaluate the curves derived from our enhancement kinetics analyses.

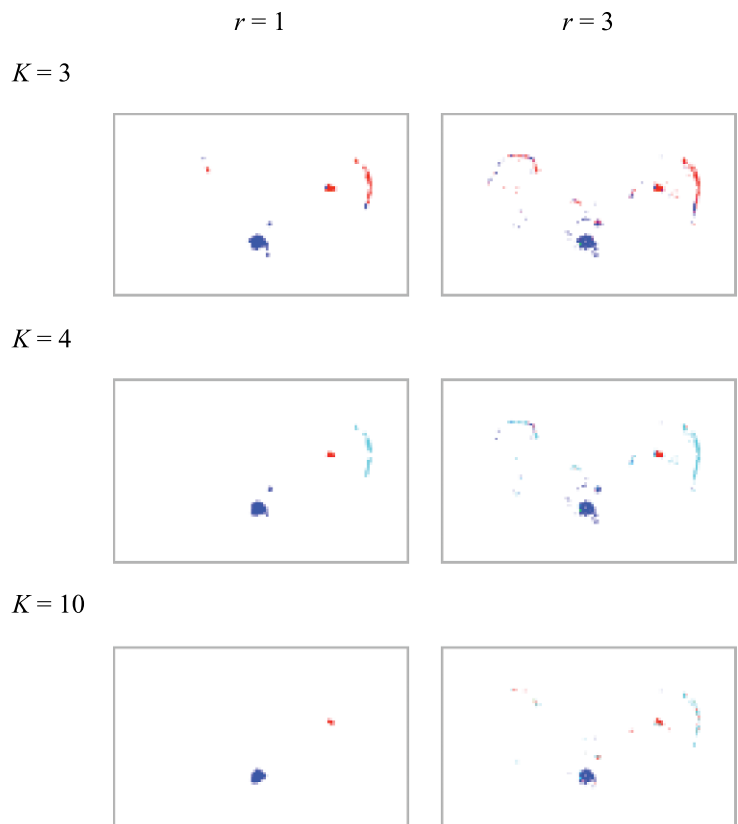
**Breast MRI Segmentation**

Figure 4 shows the segmentations for 3, 4, and 10 clusters for slice 09 and patient 05. These numbers do not include the background as a class so that the number of colors in the final-segmented images is equal to the number of clusters plus 1. This image contains a spherical lesion diagnosed as a carcinoma.

In all 3 images, one can easily recognize the heart and tumor locations. The cluster corresponding to the heart and vessels is shown in blue, whereas the tumor is in red. The remaining colors indicate other tissues. We will refer to these 3 clusters as *heart*, *tumor*, and *misc*. The latter group is composed of more than 1 cluster in the *K* = 4 and *K* = 10 cases.

In the segmentation obtained for *K* = 3 (Fig. 4B), many pixels in the skin area are classified as tumor, an indication that more classes are needed for useful image segmentation and tumor identification. This conclusion is further supported by the results for *K* = 4, in which the number of red pixels in the skin area is much smaller (see Fig. 4C), but the tumor remains solidly red.

If we compare the size (number of observations) of each cluster for *K* = 3 and *K* = 4 (Table 3), we can see that the



**FIGURE 3.** Blind restorations with *r* = 1 (first column) and *r* = 3 (second column) using images in Figure 4 as initial classifications, for *K* = 3, *K* = 4, and *K* = 10.

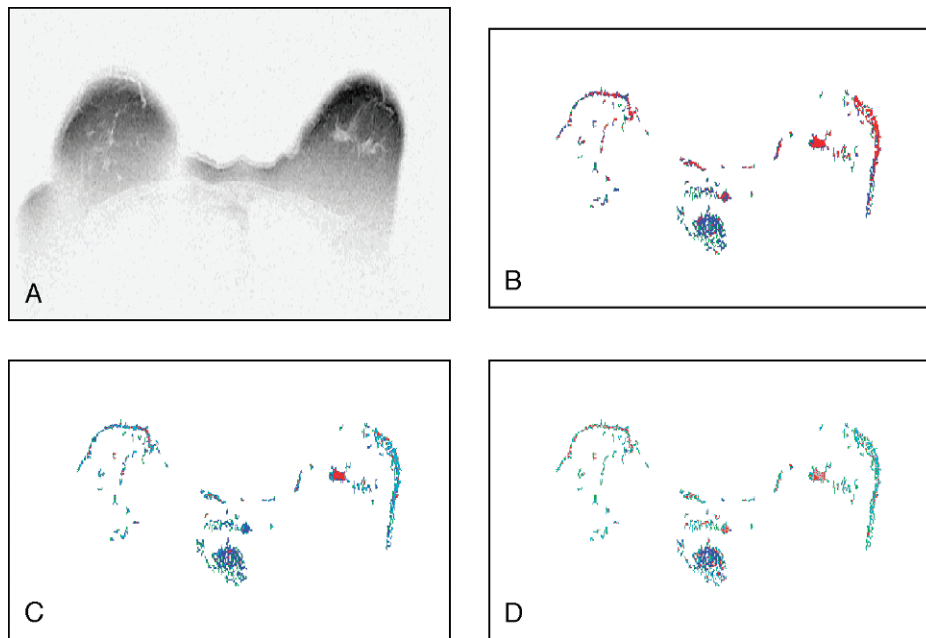


**FIGURE 4.** MCLUST classifications for patient 05, slice 09. (A) reference image, (B) 3-class segmentation, (C) 4-class segmentation, (D) 10-class segmentation.

second cluster of type *misc* and the cluster *tumor* are merged into a single one when  $K$  decreases from 4 to 3. The behavior of the 5 derived variables (see Fig. 5) in these 2 clusters is similar for the time to peak and the maximum step. The tumor shows a greater range of values for difference at peak and enhancement slope and a smaller range of values for the washout.

For both  $K = 3$  and  $K = 4$ , the main difference between the *heart* cluster and the *tumor* cluster lies in the difference at peak, enhancement slope, and washout variables. In this case, the tumor shows a greater range of values for the 3 parameters. The additional cluster produced for  $K = 4$ , referred to as *misc*<sub>1</sub>, seems to be mainly composed of outliers. The enhancement slope and the washout are equal to zero for most of the pixels in this cluster. Another difference between the segmented images for  $K = 3$  and  $K = 4$  is the classification of the area to the left of the tumor, which is classified as *tumor* for  $K = 3$  and *nontumor* for  $K = 4$ . For a higher number of clusters (Fig. 4D), the tumor area is represented by more than 1 cluster. For instance, when  $K = 10$ , 4 colors can be distinguished in this area. Note that, as before, the method detects the presence of a cluster of pixels whose enhancement slope and washout variables are equal to zero.

For  $K = 10$ , it seems also that the vessels above the heart are classified as *tumor* instead of *heart*, which does

not occur when  $K = 3$  or  $K = 4$ . Also of note is that when  $K = 4$  and  $K = 10$ , the tumor is surrounded by a thin border, composed of pixels from several clusters.

Similar analyses have been carried out for the other data sets. Figures 6 and 7 show the segmentations for patients 08 and 28. They illustrate the ability of model-based clustering to produce simple segmented images that reproduce the important features contained in the full set of 25 sequential images. In patient 08, the MR data was obtained less than a week after surgery and the radiologists concluded that there was no residual carcinoma, that is the margins of the surgery site were not suspicious. In patient 28, a spherical carcinoma is known to be present in slice 10. Note that in each case, the tumor area is not always painted red as one may wish (Figs. 6C and 7B), because in the clustering method, the color assignment is arbitrary. Hereafter, we detect the suspicious regions and automatically assign them to a predetermined color (red) using the difference at peak parameter.

The spatial techniques described in *Spatial Classification* are then applied to further refine this initial nonspatial analysis. We obtained the segmentations for  $K = 3, 4$ , and 10 shown in Figure 3 by applying blind restoration with rank  $r = 1$  and  $r = 3$  to the initial MCLUST classifications (Fig. 4). For this image, blind restoration clearly eliminates extraneous minor features and retains the tumor.

Using Bayesian morphology, we obtained the classifications shown in Figure 8.

The following are our main conclusions after carrying out similar investigations for all patients in our database:

1. Model-based clustering techniques provide informative initial segmentations.
2. Partitions into 4 colors/segments were adequate to reveal the tumor of interest. Three segments were too few because the resulting partition was not sufficient to distinguish the tumor from other tissue classes. Ten

**TABLE 2.** Curve Type Versus Pathology Results for the 19 Patients

Curve Type	Number of Patients	Pathology Results
1 (benign)	6	5 benign, 1 unknown
2 (uncertain)	5	1 unknown, 4 cancer
3 (malignant)	8	8 cancer

**TABLE 3.** Cluster Volumes for  $K = 3$  and  $K = 4$  (Patient 05, slice 09)

	Tumor	Heart	Misc <sub>1</sub>	Misc
$K = 3$	1112	1597	707	
$K = 4$	975	1312	751	378

segments were too many, because the resulting partition divided the tumor pixels among several classes.

3. Bayesian morphology is useful in refining these initial classifications by:
  - (a) giving a simultaneous (color) picture of all the (gray-level) bands;
  - (b) eliminating noise and distracting features; and
  - (c) enhancing features of potential interest.

Moderate blind restoration (second column of Fig. 3) provides much more smoothing and a clearer picture, but at

the possible cost of eliminating unclear features of potential interest. Strong blind restoration (first column of Fig. 3) smooths the image even further so that there is even more potential loss of useful information.

On the basis of these results, we recommend providing radiologists with 2 different color synthetic images, one to which statistical smoothing has been applied (eg, Fig. 8B), and another based on a more drastic heuristic smoothing method (e.g., Fig. 3, first column,  $K = 4$ ).

**ROI Analysis**

After classification, it must be decided which segments are ROIs. We based our choice on the values of the difference at peak parameter. Table 1 shows the values for the mean difference at peak and mean time to peak for the classifications shown in the first column of Figure 3. The suspicious regions, in red, are the ones selected when using a maximum mean difference at peak criterion.

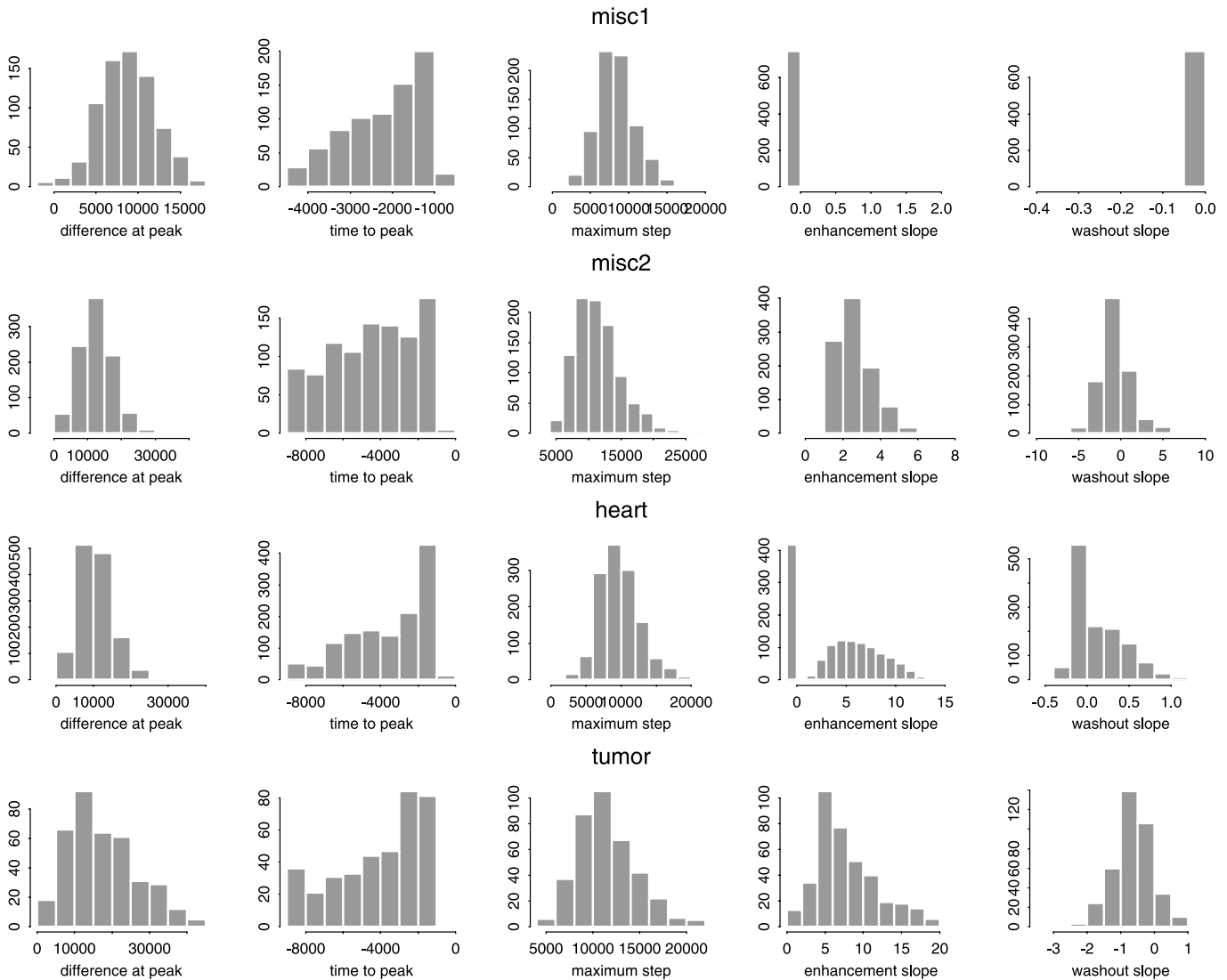


**FIGURE 5.** Histograms for the 5 parameters in the different classes of Figure 4C.



As outlined in *Enhancement Kinetics analysis*, we tried various approaches to enhancement kinetics analysis. Figures 2G–I show mean curves of all the signals within ROIs from classifications in Figures 2D–F. Figure 9 shows the mean curves in 3 different cases in which pixels were selected according to quantiles with respect to difference at peak. Figure 10 (upper curves) shows the results when pixels in the ROI were selected according to their membership probability estimates as provided by MCLUST. We also used the membership probability estimates as weights to compute a weighted mean curve (see Fig. 10, middle curves). It seems clear that using selected pixels in the ROIs according to the highest difference at peak values or the highest conditional probability provides mean curves in which features (slope enhancement, washout, etc.) are more clearly marked.

The resulting curves are usually easily assigned to one of the three curve types as described in *Distinguishing Between Malignant and Benign Lesions*. For patients 05, 08, and 28, the assignments are respectively 2, 1, and 3. This is consistent with the known respective diagnoses of a carcinoma, a benign lesion and a carcinoma, and confirms that our procedures are of interest for the differentiation between malignant and benign lesions.

The results of the analyses for all 19 patients in our database are summarized in Table 2. The known results from pathology are as follows: 12 patients have tumors determined to be carcinomas, 5 have benign lesions, and 2 have lesions whose diagnosis is uncertain. We computed some rates after the “minimum risk” strategy, that is considering doubtful lesions as malignant. We used the following parameters: (a) number of patients diagnosed as having cancer for which our method conclusion is “cancer” (*true positive*), (b) number of patients diagnosed as not having cancer for which our method conclusion is “cancer” (*false positive*), (c) number of patients diagnosed as having cancer for which our method conclusion

is “no cancer” (*false negative*), and (d) number of patients diagnosed as not having cancer for which our method conclusion is “no cancer” (*true negative*). The *sensitivity* was calculated as the number of true positive results divided by the number of patients having cancer (as given by the diagnostic information),  $a/(a + c) = 93\%$ . The *specificity* was calculated as the number of true negative results divided by the number of patients without cancer,  $d/(b + d) = 100\%$ . We also computed the probability that there is actually cancer when the analysis indicates cancer (positive predictive value):  $a/(a + b) = 1$  and that with a conclusion indicating “no cancer” there is effectively no cancer (negative predictive value):  $d/(d + c) = 0.83$ .

This level of agreement with the known results illustrates the gain in using multiple enhancement measures and in combining 2 complementary types of analysis. The classification images provide a good analysis of the different regions in the breast, with potential tumors usually emerging clearly as distinct regions. The following signal intensity time course data analysis enables us to further identify the lesion. Note that as regards the final conclusion, a detailed analysis of the classification images is not always necessary. In most cases the images make the lesion seem very clear, and our ROI selection method selects the correct region automatically.

In one case, after segmentation a region showing significant enhancement was selected. However, the location (near the patient skin) and shape of the region were such that the possibility of a malignant tumor could be discarded.

## DISCUSSION

This investigation indicates that our proposed statistical methods, which enable us to take into account more than a single enhancement measure, are quite promising for tumor

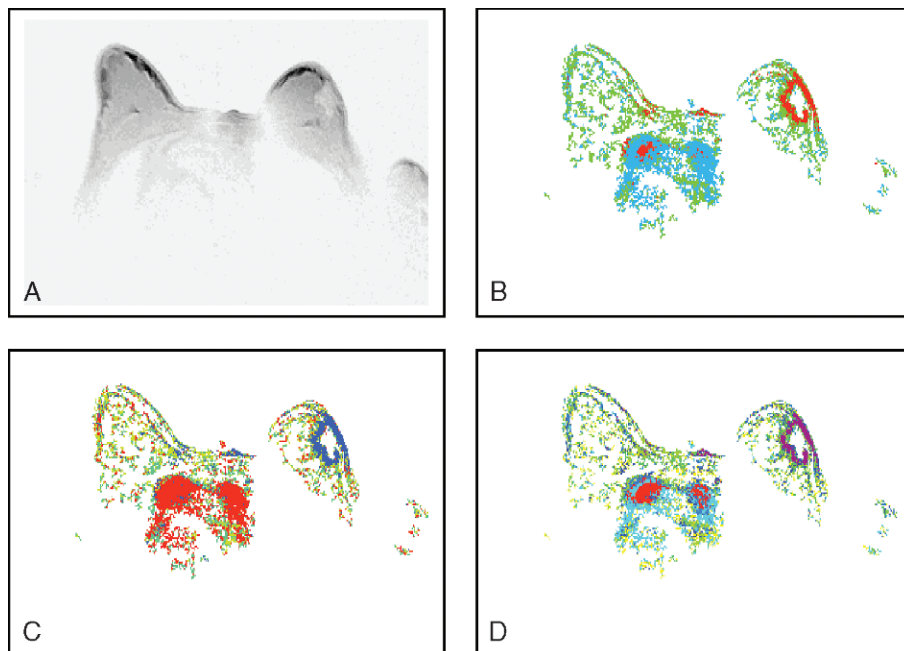


**FIGURE 6.** MCLUST classifications for patient 08, slice 06. (A) reference image, (B) 3-class segmentation, (C) 4-class segmentation, (D) 10-class segmentation.

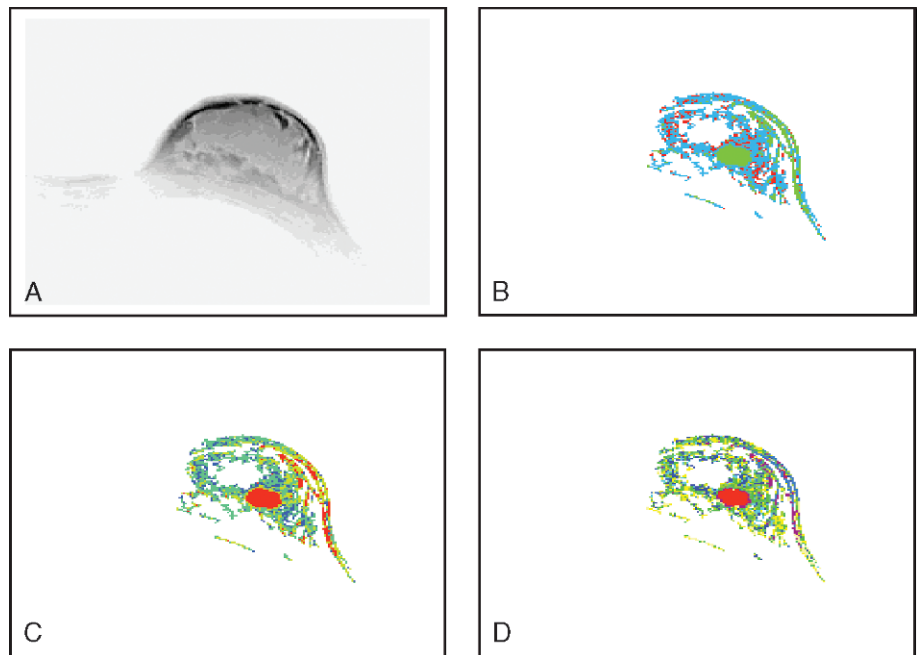


**FIGURE 7.** MCLUST classifications for patient 28, slice 10. (A) reference image, (B) 3-class segmentation, (C) 4-class segmentation, (D) 10-class segmentation.

identification. There is a clear gain in combining segmentation with kinetics analysis. Associating the location and shape of a lesion with its pattern of uptake proved to be useful in resolving questionable cases. The trade-off between smoothness and resolution needs to be assessed by further empirical research on other images. Our study is limited to the determination of feasibility for the proposed computational methods. Clinical value would have to be assessed in more extensive and controlled studies, which in the light of our initial experience may be warranted.

Other authors have addressed the issue of automatic ROI selection, though in many cases the methods require manually selected regions as input. Armitage et al<sup>29</sup> devised an optimization scheme for a model relating the MR signal to the contrast agent concentration to ensure reliable measurements, as well as color representations and vector maps of pharmacokinetic models of contrast uptake as visual aids to segmentation of malignant tumors. A recent study by Preda et al<sup>30</sup> concluded that ROIs based on the tumor periphery were better than those based on the whole tumor region in histological grade prediction.

With respect to tumor classification, Sinha et al<sup>31</sup> used linear discriminant analysis of several independent spatial

and kinetic features of MR images of breast lesions to improve classification accuracy over that of a single feature. The features included characteristics of the uptake curve, and boundary and texture of the region. Fischer et al<sup>32</sup> used prototype-based cluster algorithms to group enhancement curves, which were then summarized by a smaller set of groups using self-organizing maps (SOMs). Each group was subsequently assigned a characterizing profile or “center,” which was compared with predefined classification profiles together with an assessment of the spatial location of contributing voxels. The SOM step is fast, but needs to be done interactively because assigning enhancement profiles to clusters requires training the map before visualization. Penn et al<sup>33</sup> proposed a statistical fractal dimension feature derived from fractal interpolation function models that was able to discriminate well between benign and malignant masses in cases that were difficult to classify by experts. Nunes et al<sup>34</sup> developed a tree-based prediction model to increase specificity in dynamic MR interpretation.

de Pasquale et al<sup>35</sup> proposed Bayesian algorithms for spatiotemporal image restoration. They describe 2 different models in which the parameters are estimated by computationally intensive Markov chain Monte Carlo techniques.

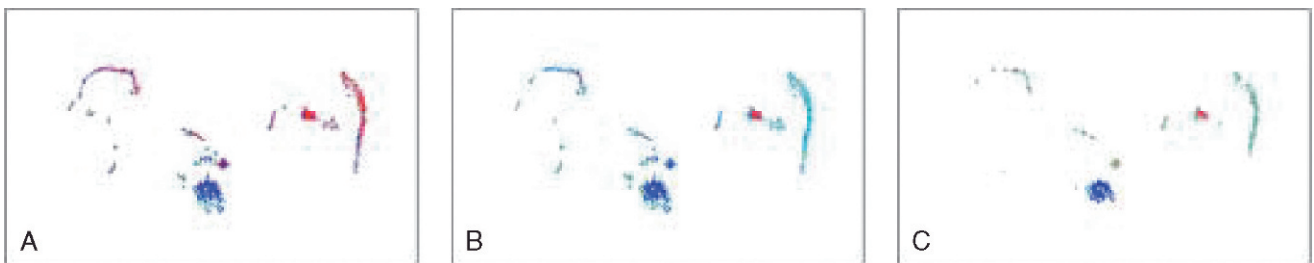


**FIGURE 8.** Bayesian morphology using images in Figure 4 as initial classifications. (A)  $K = 3$ , (B)  $K = 4$ , (C)  $K = 10$ .

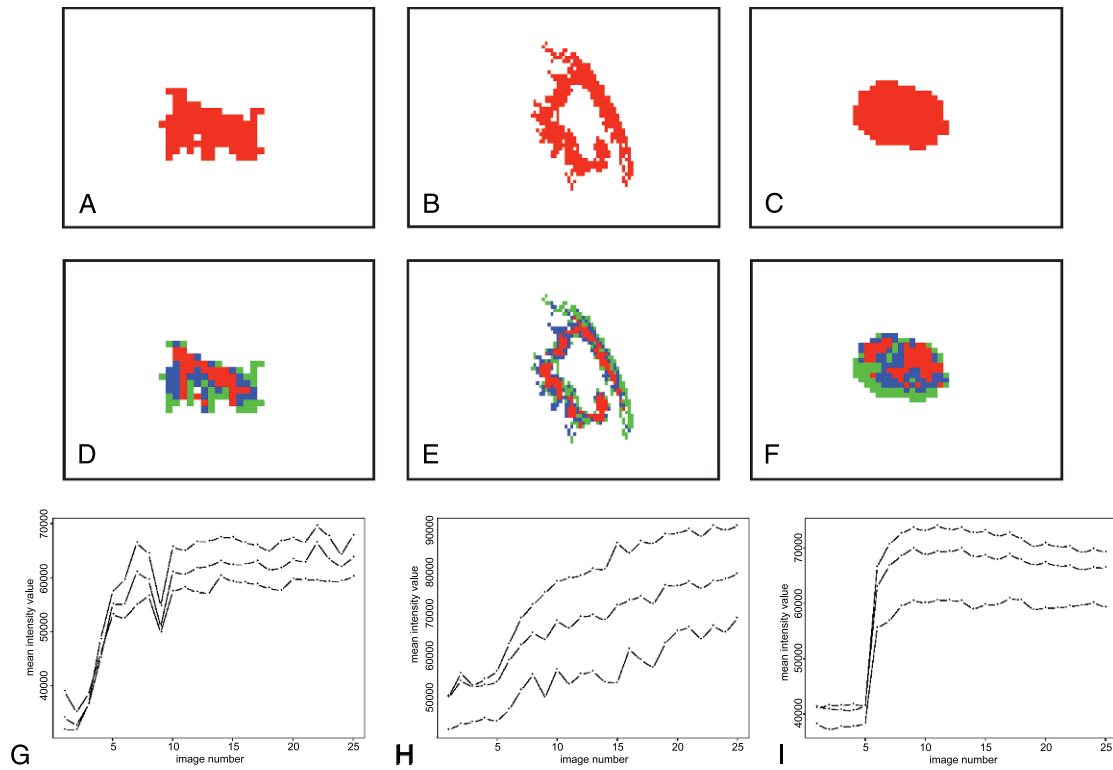


**FIGURE 9.** ROIs using 33% and 67% difference at peak quantiles, and associated mean curves in three cases. (A), (B), (C) zoomed ROIs from MCLUST classifications with  $K = 4$ , for patient 05, slice 09, patient 08, slice 06 and patient 28, slice 10. (D), (E), (F) ROI segmentations using difference at peak quantiles: highest 33% values in red, lowest 33% values in green. (G), (H), (I) mean-time intensity signals in each class (upper curve for the red class, lower curve for the green class).

Regions of interest (in which significant differences in the intensity of the image in time are present) are determined before the Bayesian analysis using a hypothesis test based on the estimated distribution of the mean variation of the image in time within a nontumorous region selected manually by the radiologist. The method was illustrated on a sequence of images obtained from 1 patient. Classification into malignant and benign pixels within the

ROI was subsequently done using univariate Gaussian models, with the number of classes is determined by the radiologist's experience and needs. A number of authors have trained neural network classifiers to various dynamic MR measurements and observations.<sup>36–38</sup>

All of the above methods for ROI classification are supervised, meaning that they rely on cases in which the diagnoses are known to develop models determining the

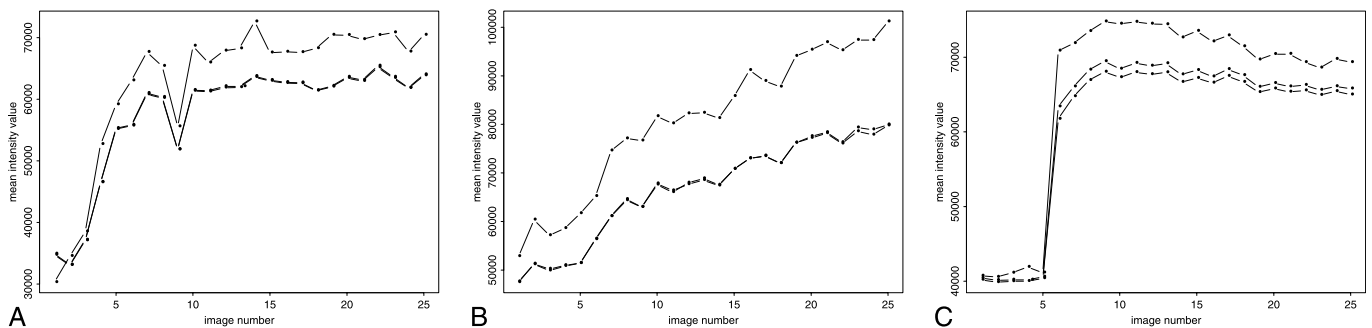


**FIGURE 10.** Mean curves using conditional probabilities estimates from MCLUST. (A) patient 05, slice 09, (B) patient 08, slice 06 (C) patient 28, slice 10. Upper curves: mean curves when selecting pixels with conditional probability very close to 1 (within  $10^{-7}$ ). Middle curves: weighted mean curves when using conditional probabilities as weights. Lower curves: mean curves using all pixels in the ROIs.

unknown cases. The method we have proposed here for ROI classification and selection is unsupervised, though a supervised analog is available.<sup>20</sup>

Various authors have also combined spatial and kinetic analyses for tumor classification. Yoo et al<sup>39</sup> used independent component analysis to delineate malignant and benign lesions, and areas with high-temporal correlations with the extract signal components were then selectively visualized. Other approaches combining quantitative signal intensity profiles with qualitative morphological features including lesion shape, margins, and enhancement patterns in pre-selected ROIs have been suggested to differentiate lesion type.<sup>40–42</sup>

Future trends for dynamic MRI include combinations with other sophisticated imaging technologies,<sup>43–45</sup> in addition to methodological improvements,<sup>46,47</sup> and those we have here proposed for dynamic MRI as a technology in its own right.

### ACKNOWLEDGMENTS

This research was supported by NIH grant 8 R01 EB002137-02, by ONR grants N00014-01-10745, N00014-96-1-0192 and N00014-96-1-0330, and by Toshiba America MRI, Inc. The authors are grateful to Leon Kaufman, David Haynor, Doug Ortendahl and Brad Wyman for useful comments and discussions, and to Andrew Jianhua Li for providing the software for computing the 5-intensity parameters from the image data.

### REFERENCES

1. Padhani AR. Dynamic contrast-enhanced MRI in clinical oncology: current status and future directions. *J Magnet Resonance Imag*. September 25, 2002;16:407–422.
2. Kneeshaw PJ, Turnbull LW, Drew PJ. Current applications and future directions of MR mammography. *Brit J Canc*. 2003;88:4–10.
3. Szabó BK, Aspelin P, Kristofferson Wilberg M, et al. Dynamic MR imaging of the breast. *Acta Radiologica*. July 2003;44:379.
4. Bluemke DA, Gatsonis CA, Chen MH, et al. Magnetic resonance imaging of the breast prior to biopsy. *J Am Med Assoc*. December 8, 2004;292:2735–2742.
5. Hylton N. Magnetic resonance imaging of the breast: opportunities to improve breast cancer management. *J Clin Oncol*. March 10, 2005; 23:1678–1684.
6. Liberman L, Menell JH. Breast image reporting and data system (BI-RADS). *Radiol Clin North Amer*. May 2002;40:409–430.
7. Chen W, Giger ML, Lan L, et al. Computerized interpretation of breast MRI: investigation of enhancement-variance dynamics. *Med Phys*. May 2004;31:1076–1082.
8. Sardanelli F. MultiHance for dynamic MR imaging of the breast. *Eur Radiol Suppl*. June 2004;14:65–70.
9. Deurloo EE, Muller SH, Peterse JL, et al. Clinically and mammographically occult breast lesions on MR images: potential effect of computerized assessment on clinical reading. *Radiology*. 2005;234:693–701.
10. Pediconi F, Catalano C, Venditti F, et al. Color-coded automated signal intensity curves for detection and characterization of breast lesions: preliminary evaluation of a new software package for integrated magnetic resonance-based breast imaging. *Invest Radiol*. July 2005; 40:448–457.
11. Pfliederer SO, Marx C, Vagner J, et al. Magnetic resonance-guided large-core breast biopsy inside a 1.5-T magnetic resonance scanner using an automatic system: in vitro experiments and preliminary clinical experience in four patients. *Invest Radiol*. July 2005;40:458–464.
12. Sampat MP, Markey MK, Bovik AC. Computer-aided detection and diagnosis in mammography. In: Bovik A, ed. *Handbook of Image and Video Processing*, 2nd ed. Academic Press; 2005:1195–1217.
13. Wells W, Grimson W. Adaptive segmentation of MRI data. *IEEE Trans Med Imag*. 1996;15:429–442.
14. Held K, Kops E, Krause B, et al. Markov random field segmentation of brain MR images. *IEEE Trans Med Imag*. 1997;16:878–886.
15. Zhang Y, Brady M, Smith S. Segmentation of brain MR images through a hidden Markov random field model and the Expectation–Maximization algorithm. *IEEE Trans Med Imag*. 2001;20:45–57.
16. Li AJ. *Streaming Data Analysis Algorithms and Implementations*. Technical report, TAMI RIL report; 1999.
17. Schwarz G. Estimating the dimension of a model. *Ann Statist*. 1978;6:461–464.
18. Kass RE, Raftery AE. Bayes factors. *J Amer Statist Assoc*. 1995;90:733–795.
19. McLachlan GJ, Peel D. *Finite Mixture Models*. Wiley; 2000.
20. Fraley C, Raftery AE. Model-based clustering, discriminant analysis and density estimation. *J Amer Statist Assoc*. 2002;97:611–631.
21. Forbes F, Raftery AE. Bayesian morphology: fast unsupervised Bayesian image analysis. *J Amer Statist Assoc*. 1999;94:555–568.
22. Dempster AP, Laird N, Rubin DB. Maximum likelihood from incomplete data via the EM algorithm (with discussion). *J R Statist Soc, Series B*. 1977;39:1–38.
23. Fraley C, Raftery AE. Enhanced software for model-based clustering, density estimation, and discriminant analysis: MCLUST. *J Classific*. 2003;20:263–286.
24. Banfield JD, Raftery AE. Model-based Gaussian and non-Gaussian clustering. *Biometrics*. 1993;49:803–821.
25. Heijmans HJ. Mathematical morphology: a modern approach in image processing based on algebra and geometry. *SIAM Rev*. 1995; 37:1–36.
26. Besag JE. On the statistical analysis of dirty pictures. *J R Statist Soc, Series B*. 1986;48:259–302.
27. Kuhl CK. MRI of breast tumors. *Eur Radiol*. January 2000;10:46–58.
28. Helbich TH. Contrast-enhanced magnetic resonance imaging of the breast. *Eur J Radiol*. 2000;34:208–219.
29. Armitage PA, Behrenbruch CP, Brady JM, et al. Extracting and visualizing physiological parameters using dynamic contrast-enhanced magnetic resonance imaging of the breast. *Med Image Anal*. August 2005;9:315–329.
30. Preda A, Turefschek K, Daldrop H, et al. The choice of region of interest measures in contrast-enhanced magnetic resonance image characterization of experimental breast tumors. *Invest Radiol*. June 2005;40:349–354.
31. Sinha S, Lucas-Quesada FA, DeBruhl ND, et al. Multifeature analysis of Gd-enhanced MR images of breast lesions. *J Magnet Reson Imag*. 1997;7:1016–1026.
32. Fischer H, Otte M, Ehrhrit-Braun C, et al. Local elastic matching and pattern recognition in MR mammography. *Int J Imag Syst Technol*. March 3, 1999;10:199–206.
33. Penn AI, Bolinger L, Schnell MD, et al. Discrimination of MR images of breast masses with fractal-interpolation function models. *Acad Radiol*. 1999;6:156–163.
34. Nunes LW, Schnell MD, Orel SG. Update of breast MR imaging architectural interpretation model. *Radiology*. 2001;219:484–494.
35. de Pasquale F, Barone P, Sebastiani G, et al. Bayesian analysis of dynamic breast images. *J R Statist Soc, Series C—Appl Statist*. August 2004;53:475–493.
36. Tzacheva AA, Najaran K, Brockway JP. Breast cancer detection in gadolinium-enhanced MR images by static region descriptors and neural networks. *Med Phys*. February 19, 2003;17:337–342.
37. Vornweg TW, Buscema M, Kauczor HU, et al. Improved artificial neural networks in prediction of malignancy of lesions in contrast-enhanced MR-mammography. *Med Phys*. 2003;30:2350–2359.
38. Lucht RE, Delorme S, Hei J, et al. Classification of signal-time curves obtained by dynamic magnetic resonance mammography: statistical comparison of quantitative methods. *Invest Radiol*. July 2005;40: 442–447.
39. Yoo S-S, Gil Choi B, Han J-Y, et al. Independent component analysis for the examination of dynamic contrast-enhanced breast magnetic resonance data: preliminary study. *Invest Radiol*. December 2002; 37:647–654.



40. Liu PF, Debatin JF, Cadaff RF, et al. Improved diagnostic accuracy in dynamic contrast-enhanced MRI of the breast by combined quantitative and qualitative analysis. *Brit J Radiol.* 1998;71:501–509.
41. Tozaki M, Igarashi T, Matsushima S, et al. High-spatial-resolution MR imaging of focal breast masses: interpretation model based on kinetic and morphological parameters. *Rad Med.* 2005;23:43–50.
42. Wiener JI, Schilling KJ, Adami C, et al. Assessment of suspected breast cancer by MRI: a prospective clinical trial using a combined kinetic and morphologic analysis. *Amer J Roentgenol.* 2005;184:878–886.
43. Jacobs MA, Barker PB, Argani P, et al. Combined dynamic contrast breast MR and proton spectroscopic imaging: a feasibility study. *J Magnet Resonance Imag.* December 20, 2004;21:23–28.
44. Vornweg TW, Teifke A, Kunz RP, et al. Combination of low and high resolution sequences in two orientations for dynamic contrast-enhanced MRI of the breast: more than a compromise. *Eur Radiol.* October 2004;14:1732–1742.
45. Choi B, Han B-K, Choe YH, et al. Three-phase dynamic breast magnetic imaging with two-way subtraction. *J Comput Aided Tomogr.* 2005;29:834–841.
46. Miyake K, Hayakawa K, Nishino M, et al. Benign or malignant? differentiating breast lesions with computed tomography attenuation values on dynamic computed tomography mammography. *J Comput Aided Tomogr.* 2005;29:772–779.
47. Woodhams R, Matsunaga K, Iwabuchi K, et al. Diffusion-weighted imaging of malignant breast tumors: the usefulness of apparent diffusion coefficient (ADC) value and ADC map for the detection of malignant breast tumors and evaluation of cancer extension. *J Compu Aided Tomogr.* 2005;29:644–649.